Based polymer nanoparticles from bee pollen attenuate non-small lung cancer through enhancement of apoptosis and cell cycle arrest in vivo

Elsayed I. Salim[1], Magdy E. Mahfouz[2], Eman A. Eltonouby[1*], Nemany A. N. Hanafy[3*] and Ezar H. Hafez[1]

*Correspondence:
dreman_ali99@yahoo.com;
nemany.hanafy@nano.kfs.edu.eg

[1] Research Laboratory of Molecular Carcinogenesis, Department of Zoology, Faculty of Science, Tanta University, Tanta 31527, Egypt
[2] Department of Zoology, Faculty of Science, Kafrelsheikh University, Kafrelsheikh 33516, Egypt
[3] Group of Bionanotechnology and Molecular biology, Department of Nanomedicine, Institute of Nanoscience and Nanotechnology, Kafrelsheikh University, Kafrelsheikh 33516, Egypt

Abstract

Bee pollen extract (BPE)-based polymer nanoparticles (BPENP) were fabricated using bovine serum albumin (BSA) and targeted with folic acid and were further characterized. Mice groups are: Group 1 received saline, whereas Groups 2, 3, 4, 5, and 6 received a single dose of urethane, followed by weekly injections of butylated hydroxy-toluene (BHT). After the BHT injection, the mice in Groups 3, 4, 5, and 6 received BPE, Avastin, BPENP, and BPENP + Avastin, respectively. The number and size of tumors were decreased in Group 6 compared to those in the other groups. The ratios of early and late apoptotic cells in Groups 3, 4, 5, and 6 (42.8%, 41.4%, 26.2%, and 45.4%, respectively) were higher than that in the untreated group. The PCNA-labeling indexes (LI)% in tissues and lesions from Group 6 were lower than those in the other groups; on the other hand, the Caspase-3 LI (%) was higher than those in the other groups. No significant differences in *HRAS* and *MAPK* levels were observed between Group 6 and the other groups. However, the level of *Bax* was significantly increased, whereas those of *Bcl2* and *P21* were decreased in Group 6 compared to those in Groups 4 and 5. According to the results of the current study's in vivo lung cancer mouse model, adjuvant chemotherapy given in conjunction with a polyphenolic substance derived from bee pollen significantly activates the apoptotic pathways as measured by flow cytometry, immunohistochemistry, and apoptotic genes. It also significantly reduces tumor volume and growth as measured by histopathology.

Keywords: Bee pollen, Nanoparticles, Lung cancer, Avastin, Apoptosis, In vivo

Salim *et al. Cancer Nanotechnology* (2023) 14:77

Page 2 of 21

Graphical Abstract
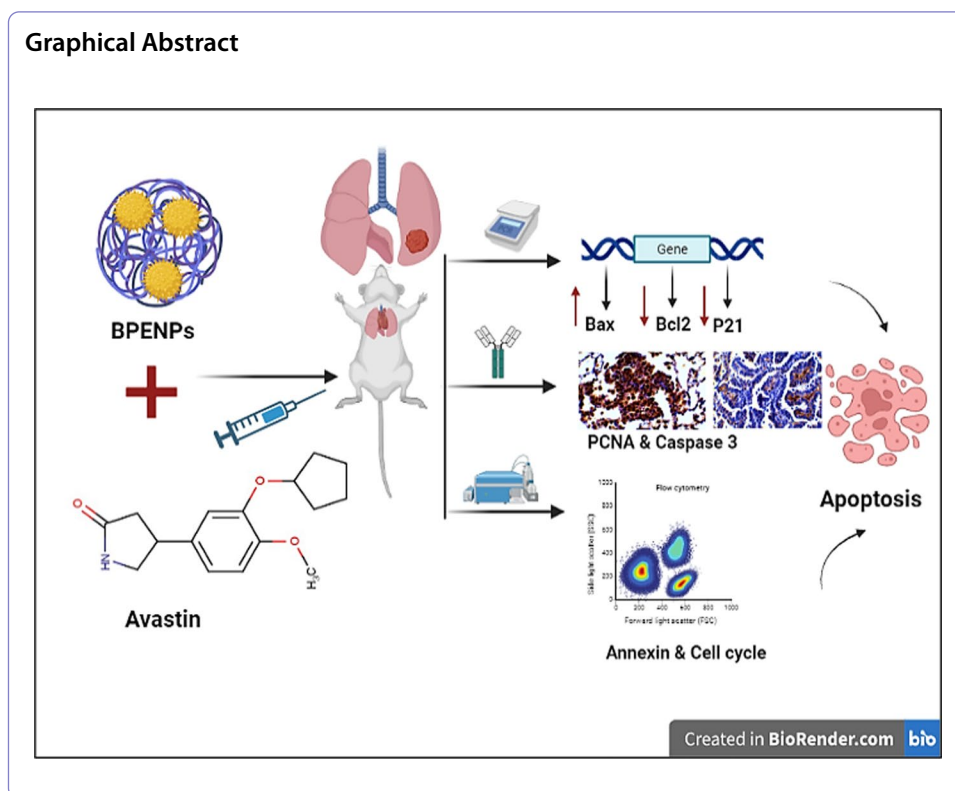
Introduction

Lung cancer account for the majority (11.4%) of malignant tumors in the world after breast cancer (11.7%) (Sung et al. 2020). The heterogeneity of the disease may be attributed to the pathologically and clinically significant subtypes. Small-cell lung carcinoma (SCLC; 12.9% of cases) and non-small-cell lung carcinoma (NSCLC; 83.9% of cases) are the two main subtypes of lung malignancies, which can be distinguished based on their primary histotypes, prognoses, and therapeutic effects (Fujimoto and Wistuba 2014). Smoking is a known primary risk factor for SCLC, the most aggressive and rapidly developing type of lung cancer (Govindan et al. 2006). The three primary subtypes of NSCLC include squamous cell lung carcinoma (SqCC), non-SqCC (often known as adenocarcinoma), and large-cell (undifferentiated) lung carcinoma (LCLC). Sarcoma-like tumors and tumors of the salivary glands account for a relatively minor portion of all cases of NSCLC (Padanad et al. 2016).

Adenocarcinoma (ADC), the most common form of NSCLC, accounts for 47.9% of all instances of lung cancer (Howlader et al. 2019). SqCC normally develops in the center and arises from the main or lobar bronchus (Travis et al. 2015). LCLCs, the least common NSCLC, account for 1.5% of all lung cancers; they are squamous cell, glandular, or small-cell non-differentiated NSCLCs that lack histological or immuno-histochemical (IHC) evidence of any differentiation (Berk et al. 2022).

Bee pollen (BP) is rounded, seed-like particles ranging from 2.5 to 5 mm in size. It is encased in a protective shell and loaded with nutrients, such as proteins, lecithin, active enzymes, folic acid, vitamins (particularly vitamin B), and other minerals. The

Salim *et al. Cancer Nanotechnology* (2023) 14:77

Page 3 of 21

physical forms of BP vary depending on the plant species. Numerous studies have shown that BP can cure obesity, allergies, and infertility (Medeiros et al. 2008). It is a potential source of flavonoids, such as hesperidin, rutin, kaempferol, apigenin, luteolin, quercetin, and isorhamnetin, and natural antioxidants, such as vanillic, protocatechuic, gallic, and p-coumaric acid (Karimi Jashni et al. 2016). These naturally occurring polyphenols have a range of actions, including anti-inflammatory, anti-carcinogenic, anti-fungal, and antibacterial activities (Ferguson 2001). In addition, the cytotoxic effects of these polyphenols on several tumor cell lines via interruption of the cell cycle or induction of apoptosis after co-encapsulation with the anticancer drugs have been previously demonstrated (Renault-Mahieux et al. 2022).

A submicron colloidal dispersion system called drug nanocrystal boosts the saturation solubility of the drug and increases its bioavailability by adding active ingredients, which are stabilized by polymers or surfactants. Polymeric nanoparticles are created when amphiphilic copolymers self-assemble into nanoparticles in water. They often have better stability, tighter size distribution, and more regulated drug release characteristics (Hu et al. 2010).

Recently, several nano-systems were to enhance the biological activity and stability of drugs when stored and consumed (Zheng et al. 2022). The purpose of this study was to demonstrate the effects of BP extract (BPE) and BPE-based polymer nanoparticles (BPENP) on lung cancer in mice chemically induced with urethane and butylated hydroxy-toluene (BHT).

Materials and methods

Chemicals for BPE encapsulation

Folic acid was purchased from Fluka-Sigma-Aldrich, St. Louis, MO, USA; 7; and ethanol was obtained from Baker Analyzed, Fisher Scientific, the Netherlands. BSA, protamine (PRM), formaldehyde, and dimethyl sulfoxide (DMSO) were purchased from Sigma-Aldrich, St. Louis, MO, USA.

BPE for the encapsulation process

The bee pollen of *Trifolium alexandrinum* (Egyptian clover; also known as Berseem), was used for extraction. In brief, 3g of dried BP powder and a flask containing 5 ml of DMSO and 45 ml of 96% ethanol were used. The mixture was stirred using a magnetic stirrer at 200 rpm for 1 h at 55 °C. The supernatant was spun for 10 min at a speed of 6000 rpm, collected, and stored as a crude extract at 4 °C until use for the creation of the nanoparticles.

BPENP preparation

The BPE (20 mL) and BSA (50 mg/50 mL) dissolved in distilled water were combined and mixed with a magnetic stirrer for 5 min at room temperature. PRM-conjugated folic acid (50 mg/100 ml) dissolved in distilled water was added to the liquid and stirred with the magnetic stirrer for 5 min. The BPENPs were dialyzed against distilled water and stored at -20 °C for lyophilization (Hanafy et al. 2023). After lyophilization, 2 g of the BPENP were dissolved in 21.5 ml of 0.09% saline resulting in 93 mg/ml saline. The mice

were given daily doses of 0.5 ml of the solution (each mouse received 46.5 mg/day in 0.5 ml solution).

Characterization of BPE and BPENP

A scanning electron microscope (SEM; JEOL JSMIT100) was used at 15 kV to characterize the BPE and BPENP. Images from a transmission electron microscope (TEM) were captured using an EOL 2100 at an accelerating voltage of 200 kV. X-ray diffraction (XRD) tests were carried out using a Shimadzu 6000-XRD X-ray diffractometer at a copper K (Cu K) radiation wavelength of $\lambda = 1.54$ Å. The potassium bromide (KBr) pellet technique and a JASCO Fourier transform infrared (FTIR)-6800 Spectrometer were used to detect the active functional groups of the produced nanoparticles in the 500–4000 cm-1 range.

Chemicals for the animal model

Urethane (97%) and BHT were obtained from Acros-Organics (New Jersey, USA), Avastin (Bevacizumab; 100 mg/4 ml) was purchased from Hoffmann-La Roche Ltd., and BP was obtained from a bee product Co. placed in Egypt.

Animals protocol

Five-week-old, male Swiss albino mice were obtained from the Holding Company for Biological Products and Vaccines (VACSERA), Giza, Egypt. The weights of the mice ranged from 18 to 20 g at arrival. The animals were housed for 2 week acclimation period before the experiment starts in plastic cages (5 per cage) in a conventional animal facility, with wood chips for bedding and a natural day/night cycle at a room temperature of 24 ± 2 °C and relative humidity of $55\% \pm 10\%$ before start. Diet and water were available *ad libitium*. Approval for the study design was obtained from the Institutional Animal Care and Use Committee (IACUC) of the Faculty of Science at Tanta University (IACUC:SCI:TU: 0129).

Experimental design

At the age of 7 weeks, a total of 152 male mice were randomly separated into six groups: Group 1 intraperitoneally (i.p) received 0.9% saline, whereas Groups 2, 3, 4, 5, and 6 received a single dose of urethane (1 mg/g, i.p), followed by 6 weekly injections of BHT (the first dose was 150 mg/kg b.wt., and the remaining five doses were 200 mg/kg b.wt.) (Salim et al. 2022). After the last BHT injection, the mice in Group 3 received 0.5 ml/mouse of crude BPE by intragastroluminal gavage (i.g.) (Abdella et al. 2009). Avastin (5 mg/kg) was i.p administered to the mice of Group 4 (Bear et al. 2015). In addition, BPENP (46.5 mg/mouse/day) in 0.5 ml saline was i.g. provided to those in Group 5 (Ragelle et al. 2012). Avastin (5 mg/kg, i.p.) along with BPENP (46.5 mg/mouse) was i.g administered to the mice in Group 6. All the treatments were given twice per week. The animals were sacrificed after 14 weeks (Scheme 1).
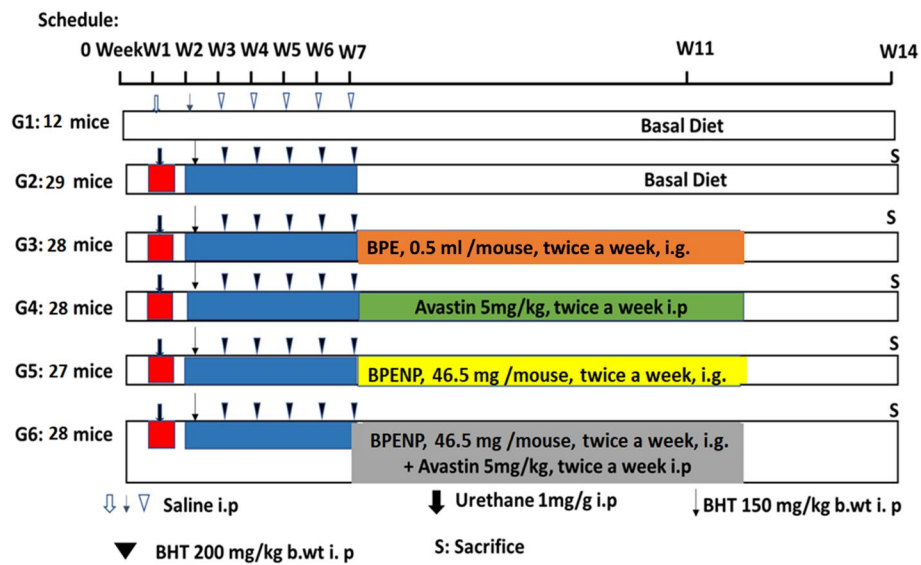
Scheme 1 The experimental design and frequency of administration

Preparation of biological samples

Diethyl ether was used to anesthetize each animal at sacrifice. After being excised from the thoracic cavity, the lungs were thoroughly cleaned with 0.09% saline, then injected with the saline solution from the tracheal opening to inflate it. After inflation, half of all lungs from each group were processed for histological and immunohistochemical analyses after fixing in 10% phosphate-buffered formalin for at least 48 h, and the diagnosis was made by two animal pathologists using the standards outlined by the mouse tumor pathology (Turosov et al. 1990). While other lung portions from at least 6 mice were immediately saved fresh for flow cytometry, other portions (from at least six different lungs) were kept at − 80 °C for the molecular and biochemical techniques.

Histopathological investigations

After embedding in paraffin and sectioned, the fixed tissues were rehydrated using a graduated series of ethanol. The slides were routinely stained with Hematoxylin and Eosin. The incidence and multiplicity (total number of nodules and cancer nodules) of the tumor and the average square areas of the nodules within an area of 1 cm^2 in the section were measured using the stage and ocular micrometer method (Salim et al. 2022), wherein the ocular micrometer was calibrated with the standard stage micrometer. The high-power objective of the ocular micrometer in a light microscope was calibrated using a stage micrometer, and the readings were consistent as long as the specific eyepiece and objective were used (Salim et al. 2022).

IHC analysis for PCNA and Caspase-3

The avidin–biotin complex method was used to visualize PCNA and Caspase-3 in 4-μm-thick sections of the lung tissues. The sections were incubated with anti-PCNA rabbit polyclonal antibody IgG (Catalog No. NBP1-89434, Novus Biologicals, USA;

dilution, 1:500) and anti-Caspase-3 rabbit polyclonal antibody IgG (Product. No. NB100-56113, Novus Biologicals, USA; dilution, 1:5000) overnight at 4°C. Subsequently, the sections were counterstained with Mayer's hematoxylin and visualized under a light microscope (Hsu et al. 1981). Briefly, sections were deparaffinized with xylene and hydrated through a graded ethanol series, rinsed in sodium citrate buffer (pH 6.0), and then were heated till boiling in an autoclave and then cooled for antigen retrieval (repeated more than once). The sections were then treated with 0.3% hydrogen peroxide and normal horse serum, The sections were then progressively treated with 0.3% hydrogen peroxide after being rinsed with TBS-T and submitted to ABC-peroxidase operations (using an ABC kit from Vector Laboratories). Normal serum was utilized as a negative control in place of the main antibodies. All IHC procedures used chromogen 3,3-diaminobenzidine tetrahydrochloride (DAB) to visualize immune complexes.

IHC evaluation and generation of labeling index (LI)

The positively stained cells for the two IHC antibodies displayed reddish-brown nuclear staining, whereas the negative cells were stained blue. Sections with no discernible brownish stain were deemed as immune-negative. The numbers of positively stained nuclei or cells from 15 to 20 high-power fields in each section were counted and divided by the total number of nuclei in each crypt X100 to generate the labeling indices (LI) for the specific antibodies (PCNA and Caspase-3). Two animal pathologists evaluated the sections in a blinded manner without being aware of the experimental groups.

Flow cytometry analysis

Aliquots of homogenate cells (about one gram in weight) from the lungs of mice from different groups were freshly suspended in phosphate-buffered saline, stored on ice, and transported to the flow cytometer equipment (fluorescence-activated cell sorting caliber flow cytometer; Becton Dickinson, Sunnyvale, CA, USA); the cytometer was equipped with a compact air-cooled low power 15 mW argon ion laser beam (488 nm) (Zaritskaya et al. 2009).

Determination of apoptosis using flow cytometry

Apoptotic and necroptotic cell death were identified by dual labeling with FITC-labeled annexin V and propidium iodide (PI). The cells in the lungs treated with BPE, Avastin, BPENP, and BPENP+Avastin were digested, washed, and resuspended in a binding solution. Then, the cells were stained with PI and annexin V-FITC and subjected to flow cytometry following a 15-min dark incubation period. The BD FACSDiva software was used to examine each sample (Becton Dickinson, USA).

Cell cycle analysis by flow cytometry

The labeling of mammalian DNA for flow cytometry was performed to synchronize the cell cycle as described previously (Vindeløv 1977). Cells from the lung tissues of mice from different groups were collected, fixed in ice-cold 70% ethanol, and left at 4 °C overnight. The next day, the cells were stained with PI (eBioscience), according to the manufacturer's recommendations, to examine the cell cycle.

RNA isolation and quantitative real-time PCR

The total RNA was isolated from the specimens using (QIAGEN, Analytik Jena Biometra AG, Berlin, Germany) and quantified using a Nanodrop 2000 (Thermo Scientific, San Jose, CA, USA). The RNA was then reverse transcribed into cDNA using the Sensiscript Reverse Transcriptase kit (QIAGEN, Germany). The following primers were used for RT-PCR: *HRAS*: forward, 5-CTCGCAGCTATGGCATCC-3; and reverse, 5-CAACGTGTG CCCTCACAG-3 *MAPK*: forward, 5-TCAAGCCTTCCAACCTC-3 and reverse, 5-GCA GCCCACAGACCAAA-3; Bcl2: forward, 5-TTGGCCCCCGTTGCTT-3 Reverse, 5-CGGTTATCGTACCCCGTTCTC-3, Bax: forward, 5-TCCCCCCGAGAGGTCTTT T-3 Reverse, 5-CGGCCCCAGTTGAAGTTG-3; P21: forward, 5-AGGTGGACCTGG AGACTCTCAG-3, Reverse, 5-TCCTCTTGGAGAAGATCAGCCG-3 *B-actin*: forward, 5-CTGTCCCTGTATGCCTCTG-3; and reverse 5-ATGTCACGCACGATTTCC-3. qRT-PCR was carried out in two-step using the SYBR GREEN PCR master mix (Quanti-Tect® SYBR® Green PCR for quantitative, real-time PCR and two-step RT-PCR using SYBR Green I kit) and the Applied Biosystems Steps One™ instrument. The amount of mRNA was calculated using the comparative CT method, which depends on the ratio of the amount of RNA from the target genes to that of the reference gene (B-actin).

Statistical analysis

Group data expressed as means ± S.D. were analyzed using the two-tailed *t* test or ANOVA analyses, while the data expressed as percentages were analyzed using the Chi-squared (X^2) analysis using the GraphPad Prism version 8.2.0 USA. $P \leq 0.05$ was considered significant.

Results and discussion

Characterization of nanoparticles

The BSA nanoparticles typically exhibited favorable properties, such as biocompatibility, biodegradability, longer plasma residence, and improved tumor dispersion (Kim et al. 2019). BSA functions as a protective colloid and remains in the bloodstream for a long time (Park et al. 2020). Protamine, protamine-based RNA delivery systems in vaccines against infectious disease and their use in cancer treatment (Ruseska et al. 2021). Folic acid was used to maintain the stability of nanoparticles and boost their adherence to cells, particularly cancer cells (Akbal et al. 2020). TEM images of BPENP in the form of a 3D assembled structure are shown in Fig. 1A–C. The average size of the nanoparticle was 25–35 nm. BP nanoparticles in the SEM image demonstrated a smooth surface and a nearly spherical form (Fig. 1D). This outcome is consistent with that reported by Keskin (2022), wherein the particle sizes of the BP-based silver nanoparticles ranged between 40 and 60 nm.

FTIR was used to detect the modifications in the chemical bands. As seen in the FTIR spectrum of BSA alone (Fig. 2A), the 3421 cm^{-1} band was assigned to the stretching vibration of the hydroxyl group, whereas the 1650 cm^{-1} band was related to amide I (mainly the C–O stretching vibrations) with a high proportion of α-helix. The band at 1512 cm^{-1} was assigned to amide II (Liu et al. 2017). The FTIR of BPE showed a broad band at 3283 cm^{-1}, corresponding to the stretching vibration of O–H-polyphenolic compounds, and two strong peaks at 2913 and 2851 cm^{-1} that were assigned to the
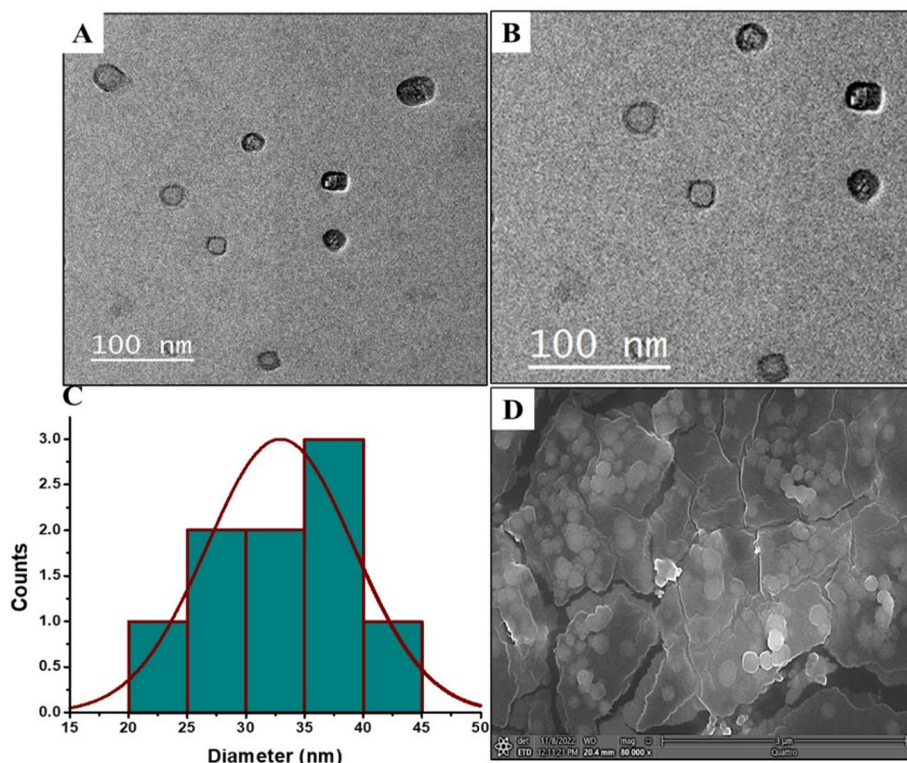
Fig. 1 A TEM images of BPENP. Scale bar, 100 nm. **B** Magnified TEM image of BPENP. Scale bar, 100 nm. **C** Histogram of the TEM images of BPENP. **D** SEM image of BPENP showing the spherical shape of the nanoparticles
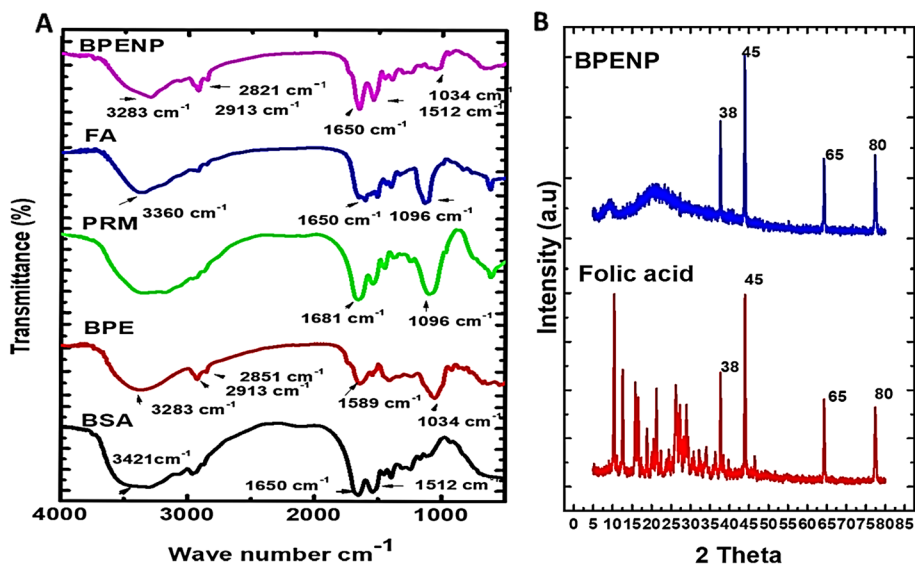

Fig. 2 A FTIR spectrum showing all the component nanoparticle fabrications. *BSA* bovine serum albumin, *BPE* bee pollen extract, *PRM* protamine, *FA* folic acid and *BPENP* bee pollen extract nanoparticles. **B** X-ray diffraction pattern of BPENP and folic acid

stretching vibration of C–H. Furthermore, the peak at 1589 cm^{-1} was associated with the C=O groups, wherein a 1034 cm^{-1} band corresponding to the stretching vibration of C–O, C–N, and C–C was detected (Swiatly-Blaszkiewicz and Pietkiewicz 2021). The FTIR of the PRM spectrum showed bands located at 1660 and 1540 cm^{-1} that were attributed to the stretching vibrations of C=O and NH–, respectively. An intense band located at 1096 cm^{-1} was assigned to the arginine of protamine (Xie et al. 2018).

The folic acid spectrum showed a strong peak at 3360 cm^{-1} associated with O–H and N–H (Fig. 2A). In addition, strong peaks at 1650 cm^{-1} were observed for the carboxylic acid groups. Likewise, a strong peak at 1096 cm^{-1} was seen due to the aromatic ring structure (Abdel-Raouf et al. 2018). The FTIR of BPENP showed a broad band at 3283 cm^{-1} corresponding to the O–H stretching vibration, and two strong peaks at 2913 and 2851 cm^{-1}, the peaks of which were assigned to the C–H stretching vibrations. Furthermore, a peak at 1650 cm^{-1} due to the presence of amide 1 in BSA and one at 1512 cm^{-1} due to folic acid, which is expressed on the phenyl and pterin ring, was observed. The 1200–500 cm^{-1} range is the so-called fingerprint region, which consists of a strong peak at 1034 cm^{-1}, corresponding to the C–O, C–N, and C–C stretching vibrations of sugar and proteins during adding PRM shifted from 1096 cm^{-1} to 1034 cm^{-1} (Singh et al. 2019).

The crystallinity of a formulation is a critical parameter that can be used to assess its physical characteristics. XRD was performed to evaluate the crystallinity of BPENP and FA by measuring the intensity in units of degree 2θ and a range of 5°–80°, as shown in Fig. 2B. The loaded folic acid nanoparticles presented with peaks at 38°, 45°, 65°, and 80° established the folic acid's crystalline form and demonstrated its effective fusion with the other components of the BPENP. In our previous work, the diffraction of pure folic acid was detected at angle 2θ = 13°, 16°, 25°, 30°, 37°, 43°, 64°, 77° (Hanafy et al. 2022).

In-life parameters

During the course of the experiment, the changes in the final body weights increased significantly in all groups compared with the initial body weights. Group 2 administered the carcinogen only showed the least growth rate among the groups, with general symptoms, such as slight hair loss, weakness, dyspnea, and hoarseness; however, this was mostly re-modulated after treatment with BPE, BPENP, or BPENP + Avastin. The growth curves of mice in all groups, mean data for initial or final body weights, and relative and absolute organ weights are represented in Additional file 1: Table S1, Fig. S1. Throughout the path of the study, on the other hand, the intervention used here did not show signs of toxicity, such as irritability (score = 0) Tremor (0), Laboured breathing (0) Staggering (0) Convulsion (0). In general, the health conditions of mice during the intervention were good, while the groups treated with crude BPE, BPENP, and Avastin were active as controls. However, some deaths occurred in both normal control and treatment groups (see Additional file 1: Table S1) due to aggressive fighting or unknown reasons.

Histopathology, incidence (%), multiplicity, and average area of the tumor

Treatment with urethane + BHT resulted in the development of several lesions (nodules) on the outer surface of the lungs, which were later identified as bronchioloalveolar adenocarcinomas, alveolar epithelial adenomas, or alveolar epithelial hyperplasia
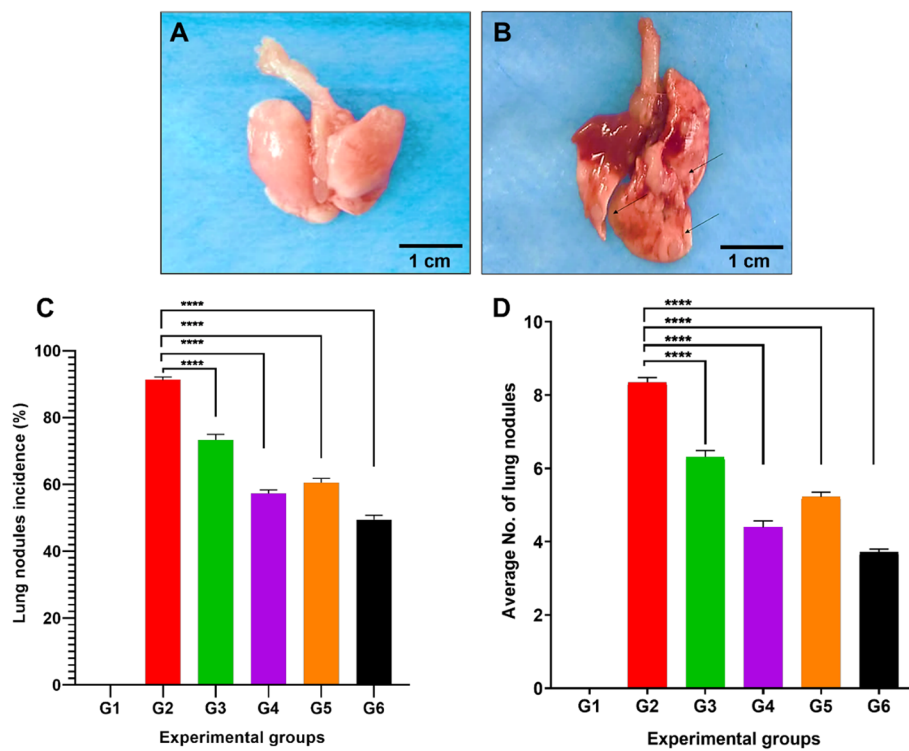
Fig. 3 Urethane + BHT-induced mouse lung nodules on the outer surface of the lung. **A** Normal lung. **B** Urethane + BHT-treated lungs with multiple focal nodules (arrows). **C** Bar graph showing the incidence of lung nodules in the six groups (no. of mouse-bearing nodules per group). **D** Bar graph showing the multiplicities of the lung nodule in all the groups (mean no. of nodules per lung). ****: significance vs. Group 2 at $P \leq 0.00001$. G1: negative control; G2: Urethane + BHT; G3: Urethane + BHT + BPE; G4: Urethane + BHT + Avastin; G5: Urethane + BHT + BPENP; G6: Urethane + BHT + BPENP + Avastin

(Figs. 3, 4). After the lungs were removed, the number of lung nodules on the surface of the lungs was counted with the naked eye. Table 1 displays the tumor incidence, number of nodules, number of tumors (multiplicity), and mean square areas of lesions within a 1 cm^2 area in the lung sections in the urethane + BHT-treated groups. The lungs in Group 1 did not present with any morphological or histological nodules. The number of nodules was marginally reduced in Group 3 after treatment with BPE and dramatically reduced in Groups 4, 5, and 6 after treatment with Avastin, BPENP, and BPENP + Avastin, respectively. On the other hand, 6.8 nodules in Group 2, which received only urethane + BHT, were identified as adenomas or adenocarcinomas. Furthermore, the average area of the lung lesions within 1 cm^2 area was 12.9 mm^2 in Group 2. The average nodule counts after treatment with urethane + BHT were 4.2 in Group 3 and 2.2 in Group 4 (diagnosed as adenoma or adenocarcinoma). The relative tumor areas were marginally lower in Group 3 and dramatically decreased in Group 4 when compared to Group 2 (Table 1).

In addition, the incidence and number of tumors in Groups 5 and 6 were considerably reduced compared to those in Group 2. Likewise, the average tumor areas in Groups 5 and 6 (6.7 mm^2 and 3.2 mm^2, respectively) were significantly lower than that in Group 2. Group 6 demonstrated a markedly reduced inhibitory response to
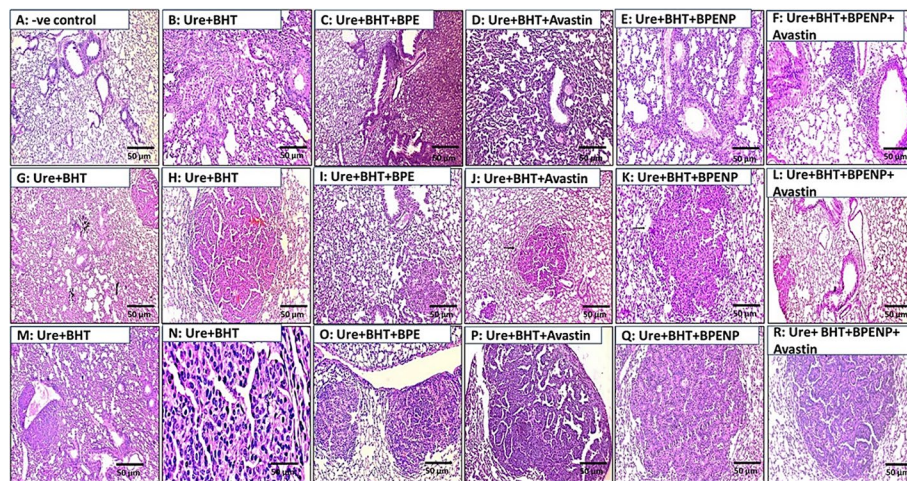
Fig. 4 Photomicrographs showing the histology of the lung epithelium and tumors in the six groups of mice. **A** Normal mouse lung epithelium from Group 1 (G1). **B** Alveolar epithelial hyperplasia from Group 2, which was administered with the carcinogen only. Increased thickness of the alveolar epithelial cells is seen in the lesion when compared to the normal lung epithelium. **C**, **D** Lung epithelium from Groups 3 and 4, which were treated with BPE and Avastin, respectively. **E** Lung epithelium from Group 5, which was treated with BPENP. **F** Lung epithelium from Group 6, which was treated with BPENP + Avastin. The thickness of the hyperplastic alveolar epithelium was reduced after all the treatments, particularly in Group 6, when compared to that in the normal control (Group 1). **G** Bronchioloalveolar adenoma from Group 2. **H** Magnified view of an area from G. The sizes of the adenomas were reduced after the treatment with BPE (**I**), Avastin (**J**), BPENP (**K**), or BPENP + Avastin (**L**). **M** Bronchioloalveolar adenocarcinomas from Group 2. **N** magnified view of an area from M. Treatment with BPE (**O**), Avastin (**P**), BPENP (**Q**), or BPENP + Avastin (**R**) reduced the sizes of the adenocarcinomas compared to that in Group 2

Table 1 Histological incidence (%), multiplicity, and average tumor area per 1 cm^2 of the lung tissue

Groups	Treatment	Mice (*n*)	No. of lung tumors [a]	Tumor incidence (%)	Tumor Multiplicity (Number of tumors/1 cm^2) [b]	Average tumor areas/1 mm^{2} [c]
G1	Control -ve	9	0	0	0	0
G2	Ure + BHT	10	8.40 ± 0.12	9/10 (90%)	6.88 ± 4.2	12.99 ± 13.8
G3	Ure + BHT + BPE	8	6.25 ± 0.17*	6/8 (75%)	4.28 ± 2.2*	7.6 ± 3.1*
G4	Ure + BHT + Avastin	12	4.58 ± 0.17*	7/12 (58.3%)	2.25 ± 2.22*	4.98 ± 6.4 *
G5	Ure + BHT + BPENP	10	5.20 ± 0.12*	6/10 (60%)	3.85 ± 3.7*	6.78 ± 5.8*
G6	Ure + BHT + BPENP + Avastin	8	3.75 ± 0.08*	4/8 (50%)	1.80 ± 1.0*, **,***	3.25 ± 4.3 *, **,***

n, number of animals used in histopathological analysis; Ure, urethane; G1: normal control; G2: Ure + BHT; G3: Ure + BHT + BPE; G4: Ure + BHT + Avastin; G5: Ure + BHT + BPENP; G6: Ure + BHT + BPENP + Avastin. **a** lesions: total microscopical (histological) lesions in lung tissues in tumor-bearing mice regardless of histological type; **b** Number of lesions histologically diagnosed as adenomas and adenocarcinomas in 1cm2 of lung tissue; **c** Areas (mm^2) (tumor size) in 1cm^2 of lung tissues; Values are means ± standard deviation (S.D.). *****: Significant vs. G2 at *P* < 0.05; ******: significant vs. G4, *******: significant vs. G5 at *P* < 0.05

combination therapy compared to the other treatment groups (Table 1). To the best of our knowledge, this is the first study to demonstrate the effect of BPE, BPENP, and BPENP + Avastin in lung cancer in vivo. However, other research combining NP and flavonoids (Parashar et al. 2018) was consistent with the present findings, which suggested that co-therapy is superior to individual therapy for improving therapeutic efficacy. Flavonoid also supports the development of a safe, effective, and targeted

Salim *et al. Cancer Nanotechnology* (2023) 14:77

Page 12 of 21

delivery system for the treatment of lung cancer using gefitinib (Gnb) and naringenin (Nar), both of which have been studied for their potential therapeutic and synergistic effects against lung cancer; co-administration of Gnb and Nar nanoparticles showed a substantial decrease in tumor volume (Saisavoey et al. 2021).

Flow cytometry analysis data for Annexin

As shown in the dot plots of the log data from the flow cytometry analysis, the percentages of annexin V-FITC-positive early and late apoptotic cells in the
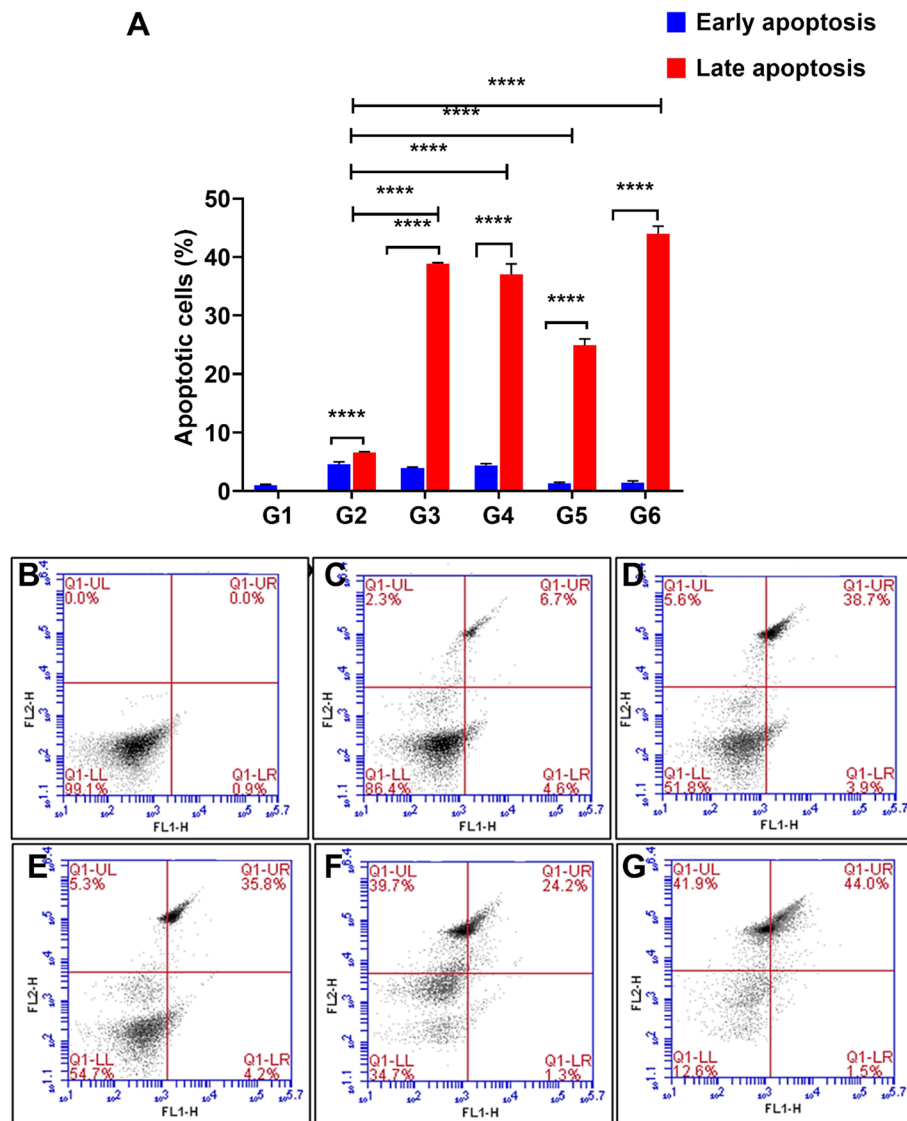
Fig. 5 Flowcytometric analysis data for annexin V staining ($n = 6$). **A** Dot plot flow cytometry analysis data showing the expression of annexin V in Groups 1–6. Values are shown as percentage means $\pm$ S.D. ****: significant vs. the next column of each other and the treated groups vs. G2 at $P \leq 0.00001$. **B** Control -ve (G1); **C** G2 (urethane + BHT); **D** G3 (urethane + BHT + BPE); **E** G4 (urethane + BHT + Avastin); **F** G5 (urethane + BHT + BPE-NP); **G** G6 (urethane + BHT + BPE-NP + Avastin). FL1-H: Annexin, FL2-H: Propidium iodide; LL: (lower left) negative for both annexin V and propidium iodide; LR: (lower right) positive annexin (early apoptosis); UL: (upper left) positive for propidium iodide (necrosis); UR: (upper right) positive for both (late apoptosis). FL2-H = Propidium Iodide fluorescence)

urethane + BHT-treated Group 2 were considerably higher than those in the negative control group (Fig. 5). Treatment with BPE, Avastin, BPENP or Avastin + BPENP in Groups 3, 4, 5, and 6 showed a significant increase in the early and late apoptotic cell numbers when compared to the urethane + BHT (Group 2) (Fig. 5).

According to Saisavoey et al. (2021), the observed underlying mechanisms, such as the stimulation of apoptosis, inhibition of cell proliferation in several cell lines, and reduction in tumor growth, account for the anticancer effects of BP.
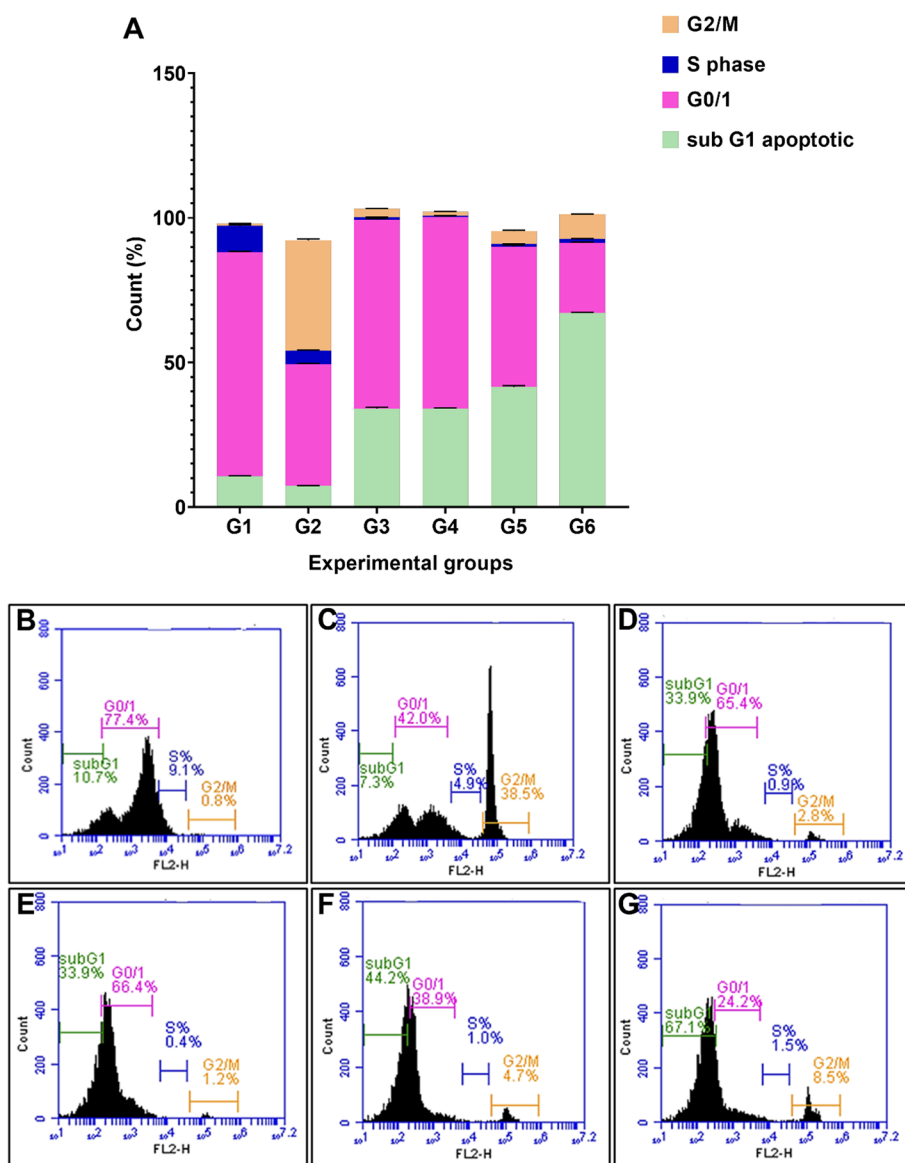
Fig. 6 Cell cycle analysis and percentage of apoptotic cells by flow cytometry (n = 6). **A** Graph showing the ratios of the various phases of the cell cycle in the six groups. Values are represented as percentage means ± S.D. ****: significant vs. G2 at $P \le 0.00001$. Sub-G1, apoptosis; G0/1, first gap phase; S phase, G2/M; M, Mitosis. **B** Control − ve (G1); **C** G2 (urethane + BHT); **D** G3 (urethane + BHT + BPE); **E** G4 (urethane + BHT + Avastin); **F** G5 (urethane + BHT + BPENP); **G** G6 (urethane + BHT + BPENP + Avastin). FL2-H = Propidium Iodide fluorescence

Cell cycle analysis data by flow cytometry

The mean numbers of subG1 apoptotic cells in Groups 3, 4, 5, and 6 were obviously greater than those in Group 2 (Fig. 6). The combination treatment with BPENP + Avastin in Group 6 showed the highest induction levels of subG1 cells (66.9% increase vs. Group 2) as compared with the other treatments in G3–G5). On the other hand, the initial gap phase (G0/1) in Group 2 was significantly lower than that in the control group (Group 1); however, this phase was substantially longer in Groups 3, 4, and 5 but less in Group 6 when compared to that in Group 2. The G0/1 phase in Group 6 was significantly less than that in Groups 3–5 probably due to the increase in the subG1 phase cells in Group 6. Furthermore, the S phase cell numbers in Group 2 were significantly lower than that in Group 1; this phase was significantly lower in Groups 3, 4, 5, and 6 than in Group 2 indicating less cellular proliferation. Group 6 showed significantly fewer S phase cell numbers than the other treatment groups. The mitotic phase (G2/M) cell numbers in Group 2 were significantly higher than that in the control (Group 1). Treatment in groups 3, 4, 5, and 6; slightly increased the numbers of cells in the G2/M phase, albeit without statistical significance. According to Khan et al. (2021) ROS can cause apoptosis by controlling the transcription of a number of redox-sensitive signal proteins. However, some flavones may also cause apoptosis by stopping the cell cycle in an ROS-independent manner at the G2/M phase.

PCNA IHC levels in lung tissues and tumors

Reddish-brown nuclear staining was seen in the lung tissues and tumors after IHC labeling for PCNA. The lung parenchyma of mice in Group 2 showed a significant increase in the number of positively stained nuclei when compared to those in Group 1 (Fig. 7). In addition, the PCNA LI (%) in Groups 3, 4, 5, and 6 were considerably lower than that in Group 2, with Group 6 showing the lowest levels. Furthermore, the PCNA LI (%) in the tissues and lesions of mice belonging to Group 6 were significantly lower than those in Groups 3, 4, and 5. These findings are consistent with that reported by Granja et al. (2016), wherein the anti-tumor effects of green tea and EGCG nanoparticles were demonstrated in vivo by assessing the levels of Ki-67, PCNA, and CDK4 in the tumor tissues. In the recent study by Salim et al. (2022) decreases in the incidence and size of the urethane + BHT-administered lung tumors in mice were followed by a dose-dependent decline in cell proliferation and PCNA LI (%) after treatment with balanitoside as adjuvant therapy. Previous studies have also reported a gradual increase in PCNA LI (%) during lung carcinogenesis.

Caspase-3 IHC levels in lung tissues and tumors

A significantly higher number of strongly positive Caspase-3-stained nuclei were seen in the lung parenchyma of mice in Group 2 when compared to that in Group 1 (Fig. 8). In addition, the lung parenchyma and lesions of mice in Groups 4, 5, and 6 showed a significant higher Caspase-3 LI (%) than those in Group 2, particularly mice of Group 6 presented the highest Caspase-3 LI (%) as compared to those from Groups 3, 4, and 5.
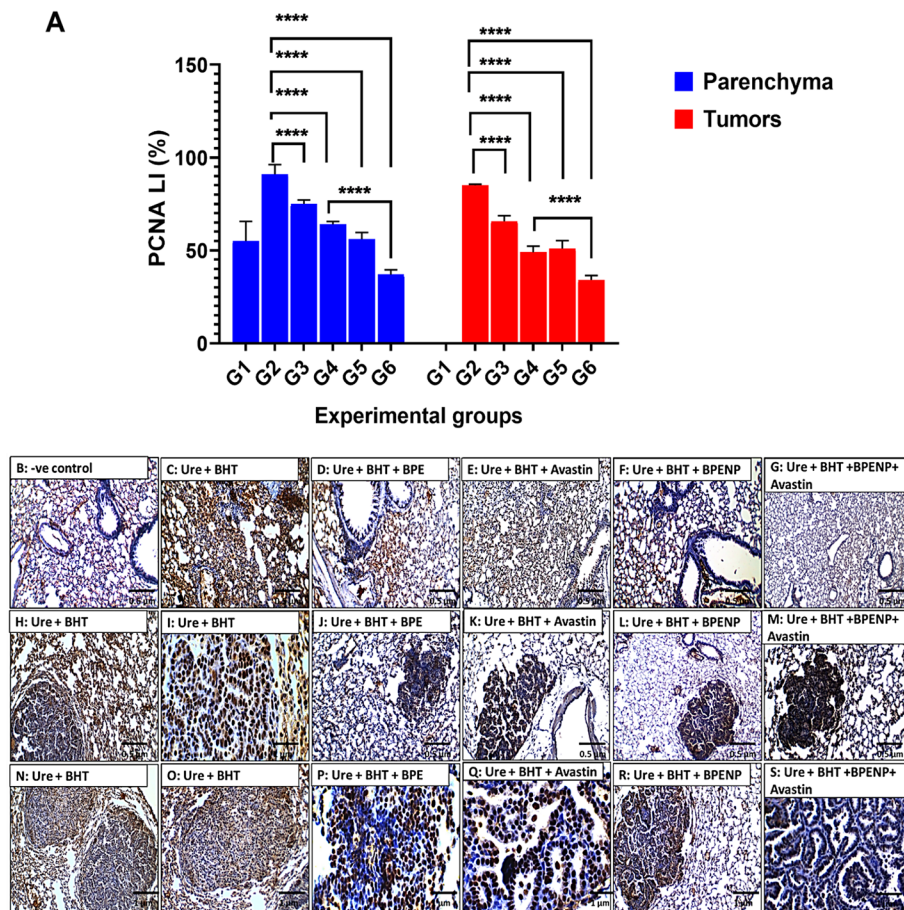
Fig. 7 PCNA staining in lung epithelium and neoplasia. **A** Bar graph of PCNA LI (%) data from the lung parenchyma and tumors (adenoma/carcinoma) in the different groups; ****: significance vs. G2 at $P \leq 0.00001$; ****: significant vs. G6 at $P \leq 0.00001$; B–S: photomicrographs showing PCNA IHC staining patterns in the different groups. **B** Normal mouse lung epithelium from Group 1 showing low PCNA IHC staining affinity; **C** alveolar epithelial hyperplasia from Group 2 with a marked increase of PCNA immunostaining **D, E** lung epithelium from Groups 3 and 4 treated with BPE and Avastin, respectively; **F** lung epithelium from Group 5 treated with BPENP; **G** lung epithelium from Group 6 treated with BPENP + Avastin. Notice the reduced thickness of the alveolar epithelial hyperplasia after all treatments, particularly in Group 6, compared to the normal control. **H** Bronchioloalveolar adenoma from Group 2, **I** magnified portion of G. Notice the reduced size of the adenomas after the treatment with BPE **J** Avastin **K** BPENP (**L**), or both (**M**). **N** bronchioloalveolar adenocarcinomas from Group 2; **O** a magnified portion of M. Treatment with BPE (**P**), Avastin (**Q**), BPENP (**R**), or both (**S**) reduced the sizes of the adenocarcinomas when compared to that in Group 2. PCNA

Lung tissues stained with Caspase-3 showed reddish-brown nuclear staining. Ben Bacha et al. (2020) reported that the anti-inflammatory properties of BPE decreased levels of IFN-γ, inhibited the apoptotic cascade, lowered the concentration of p53, and ultimately reduced the production of Caspase-3, this is consistent with the present findings.

qRT-PCR data analysis

Gene expression levels of HRAS, MAPK, Bcl2, Bax, and p21 in the lung tissues

The normalized mRNA expression levels of *HRAS* and *MAPK* did not differ substantially among the groups (Fig. 9A, B). Compared to the negative non-treated control
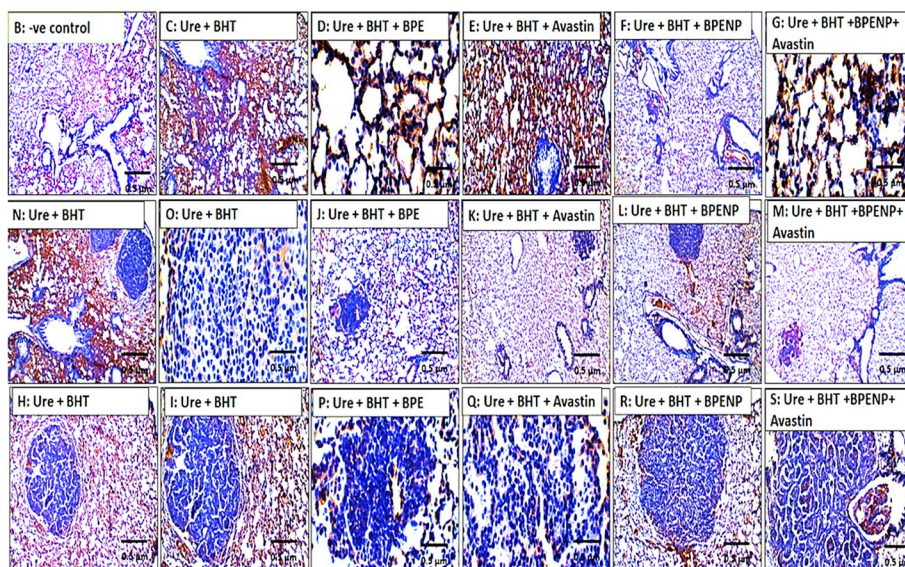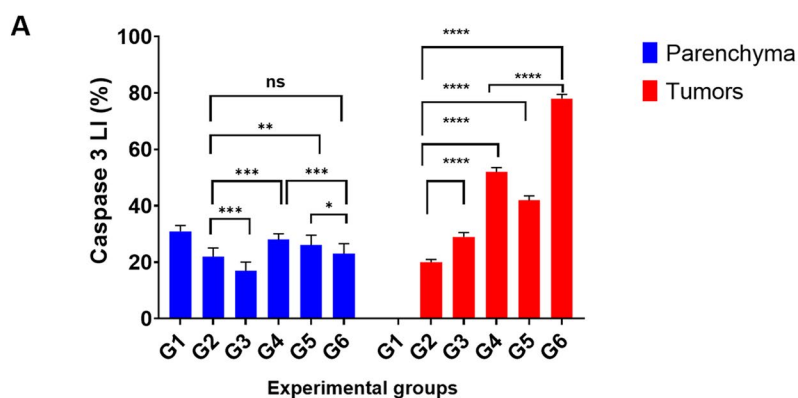
Fig. 8 Caspase-3 staining in lung epithelium and neoplasia. **A** Bar graph of Caspase-3 LI (%) in the lung parenchyma and tumors (adenoma/carcinoma) of mice in the different groups. *: significance vs. G6 at $P \leq 0.05$; **: significance vs. G2 at $P \leq 0.001$; ***: significance vs. G2 at $P \leq 0.0001$, ****: significant vs. G2 at $P < 0.00001$. **B–S** Photomicrographs showing Caspase-3 IHC staining patterns in different groups; **B** normal mouse lung epithelium from Group 1 showing low Caspase-3 IHC staining affinity; **C** alveolar epithelial hyperplasia from Group 2 with a marked increase of Caspase-3 immunostaining; **D, E** lung epithelium from Groups 3 and 4 treated with BPE and Avastin, respectively; **F** lung epithelium from Group 5 treated with BPENP; **G** lung epithelium from Group 6 treated with both BPENP and Avastin. Notice the reduced thickness of the alveolar epithelial hyperplasia after all treatments, particularly in Group 6, compared to the normal control. **H** Bronchioloalveolar adenoma from Group 2, **I** a magnified portion of G. Notice the reduced size of the adenomas after the treatment with BPE (**J**), Avastin (**K**), BPENP (**L**), or both (**M**). **N** Bronchioloalveolar adenocarcinomas from Group 2; **O** magnified portion of M. The treatment with BPE (**P**), Avastin (**Q**), BPENP (**R**), or both (**S**) reduced the adenocarcinoma sizes when compared to that in Group 2

group 1 and the positive control group 2, the normalized mRNA expression level of the *Bax* gene was significantly increased (P < 0.05) by 4.8-, 2.3-, 2.2-, and 3.3-fold in Groups 3, 4, 5, and 6, respectively (Fig. 10A). Treatment with BPENP (Group 5) considerably reduced the mRNA expression levels relative to that in Group 3 by around 2.2-fold; however, the level was statistically different from that in the normal control. Treatment with BPENP + Avastin (Group 6) significantly increased the mRNA expression levels of *Bax* by 3.3-fold when compared to the data of Group 2.
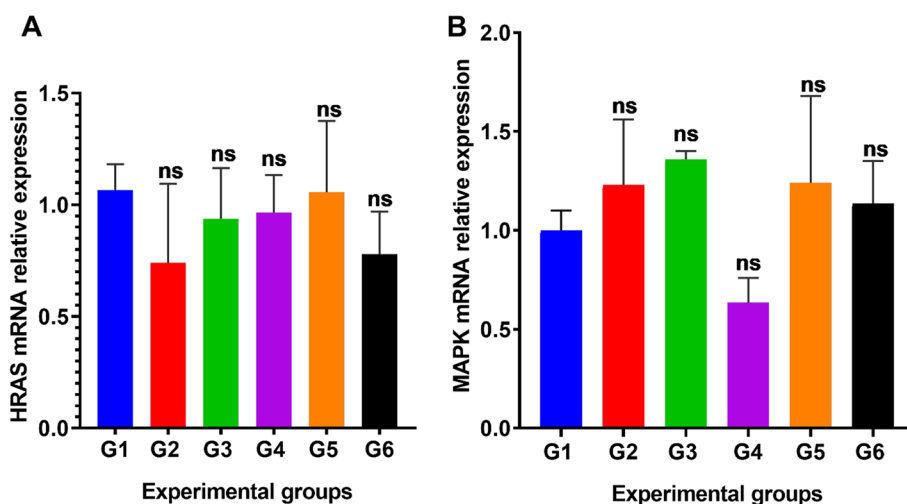
Fig. 9 qRT-PCR analysis data of the mRNA expression in different experimental groups normalized relative to *B-actin* endogenous housekeeping gene. C_T Threshold cycle. **A** *HRAS*. **B** *MAPK*. *ns* significant vs. Group 1. C_T Threshold cycle, *RQ* Real-time quantitative PCR
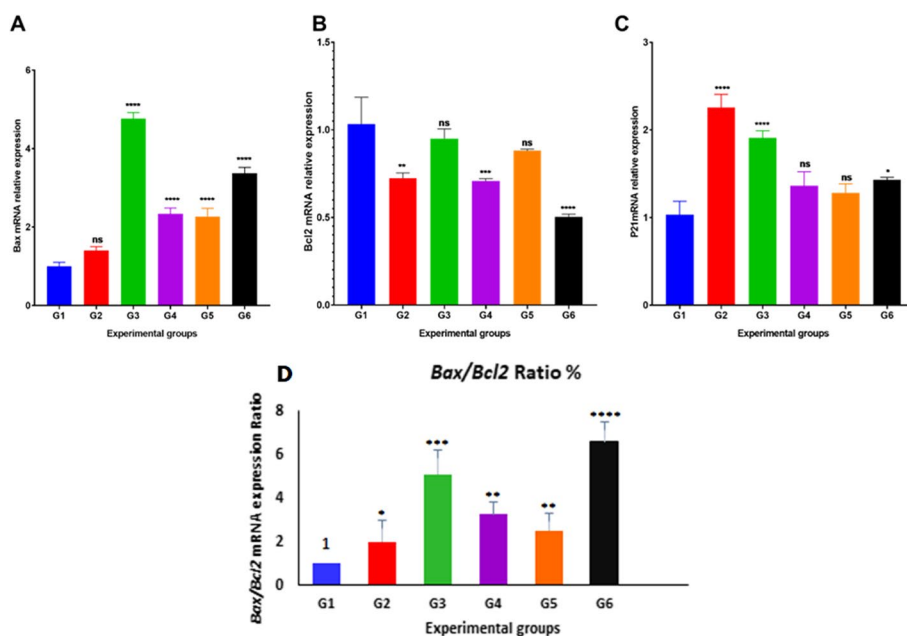

Fig. 10 qRT-PCR analysis data of the mRNA expression data in different lung mouse experimental groups normalized relative to *B-actin* endogenous housekeeping gene. C_T: threshold cycle. **A** *Bax*. **B** *Bcl2*. **C** *P21*. **D** *Bax/Bcl2* ratio. ns: non significant vs. Group 1; *: significant vs. Group 1 at $P \leq 0.05$; **: significance vs. G1 at $P \leq 0.001$; ***: significance vs. G1 at $P \leq 0.0001$, ****: significant vs. G1 at $P < 0.00001$; C_T threshold cycle, *RQ* real-time quantitative PCR

The normalized mRNA expression levels of the *Bcl2* gene were significantly down-regulated ($P < 0.05$) in Groups 2, 4, and 6 (by 0.73-, 0.71-, and 0.5-fold, respectively) compared to the control group (Fig. 10B). Treatment with BPE (Group 3) and the combination of BPE and urethane + BHT (Group 6) significantly reduced the mRNA expression levels relative to those in Group 2 by around 0.96- and 0.5-fold, respectively;

however, the levels remained significantly different from those in Group 1. Treatment with BPENP + Avastin (Group 6) resulted in a 0.5-fold drop in the mRNA expression levels of *Bcl2* when compared to those in Groups 4 and 5 (Fig. 10B).

The normalized mRNA expression levels of the *P21* gene were found to be significantly (P < 0.05) elevated in Groups 2, 3, and 6 by 2.2-, 1.9-, and 1.4-fold, respectively, when compared to those in the negative non-treated control group 1 (Fig. 10C). The levels of the gene in Groups 3, 4, 5, and 6 were significantly lower than those in Group 2 and remained significantly different from those in Group 1. BPENP treatment resulted in a significant decrease in the level of *P21* compared to that in Group 3 (Additional file 1: Figs. S2 and S3). The *Bax/Bcl2* ratio was found elevated significantly in all treatment groups, while it was most significant in Group 3 and Group 6 (Fig. 10D).

The pro-apoptotic gene *Bax* is the primary apoptosis regulator that initiates apoptosis in cells. The anti-apoptotic gene *Bcl2* can prevent apoptosis by inactivating Bax. Consequently, the Bax/Bcl2 transcription ratio can affect the growth or inhibition of cancer cells (Khodapasand et al. 2015). Naseri et al. (2021) investigated the effect of BP on the expression of the pro-apoptotic (*Bax* and *Caspase-3*) and anti-apoptotic (*Bcl-2*) genes; they demonstrated increased expression levels *of Bax, Caspase-3, -8,* and *-9* and decreased levels of *Bcl-2, Ki-67, CD31,* and *VEGF.* In another study by Zakhireh et al. (2022), the mRNA expression level of *Bax* was dramatically increased ($P \leq 0.05$), whereas that of *Bcl2* was significantly downregulated ($P \leq 0.05$) in cells seeded on PShs/Fe3O4NPs when compared to those in bare PShs. Cells cultivated on a substrate containing the highest concentration of Fe3O4NPs had the highest *Bax/Bcl2* ratio. Increased expression of *Caspase-3* and an increase in the *Bax/BCL2* ratio revealed that the intrinsic mitochondria-dependent pathway mediates apoptosis by Fe3O4NPs. Similarly, our previous results confirmed the present finding that bioactive materials isolated from bee pollen have potential therapeutic effects on non-small lung cancer cell lines (Hanafy et al. 2022).

Although the retrospective assessments of preclinical intervention studies in animal models of various diseases show that only a tiny proportion of therapies claiming positive benefits are clinically effective, the majority of therapeutic drugs currently used in clinical practice were initially created and studied in animal models to ascertain drug toxicity and safety, dosage responses, and efficacy (Koboziev et al. 2011). Thus, finding the most pertinent mice models and pharmacologic approaches to lung cancer that most closely resemble clinical conditions is one possible method to uncover novel therapies that may have a decent chance of success in carefully monitored clinical trials (Kumar et al 2022; Kwon and Berns 2013).

The current study proved that the lung cancer mouse model used here was suitable and indispensable as it validated putative driver lesions and gained insight into their mechanisms of action. This model permits mimicking many of the prominent features of human lung tumors and enabled a clear valuation of the contribution of distinct tumor characteristics such as cellular proliferation, apoptosis, enzymatic activity, or gene expression with the response to treatment. In this context, gross observations were recorded concerning the behavioral characteristics, general health, and growth rates, besides blood biochemistry, and absolute and relative organ weights revealing no toxicity or side effects during the intervention. The results ensured that this animal model represents a pharmacological

approach with a well-defined critical evaluation that is compatible with the study design and final data interpretation of this preclinical study.

Conclusion

The in vivo lung cancer mouse model in the current study revealed that adjuvant treatment with chemotherapy combined with a polyphenolic compound isolated from bee pollen significantly activates the apoptotic pathways as evaluated by flow cytometry, immunohistochemistry, and apoptotic genes, as well, it decreased the tumor volume and growth as determined by histopathology. It can be concluded that the hybrid polymeric protein nanoparticles involving natural bioactive materials, can be recommended strongly to be adjuvant with chemotherapy to potentiate its effect and minimize its required dose to diminish its toxicity on healthy cells.

Abbreviations

ANOVA	Analysis of variance
Avast.	Avastin
BPE	Bee pollen extract
BPENP	Bee pollen extract nanoparticles
DMSO	Dimethylsulfoxide
NPs	Nanoparticles
NSCLC	Non-small cell lung cancer
SCLC	Small cell lung carcinoma
ADC	Adenocarcinoma:
SqCC	Squamous cell lung carcinoma
LCLC	Large cell lung cancer
TTF1	Thyroid transcription factor 1
IHC	Immunohistochemistry
Ure	Urethane
BHT	Butylated hydroxytoluene (BHT)
Ros	Reactive Oxygen species
PCNA	Proliferating cell nuclear antigen
PI	Propidium iodide
FACS	Fluorescence-activated cell sorting
RT-PCR	Real-time-polymerase chain reaction
SD	Standard deviation
XRD	X-ray diffraction
FTIR	Fourier Trans
CS	Cationic chitosan
PLGA	Poly(lactic-co-glycolic acid)
HRAS	Harvey Rat sarcoma virus
MAPK	Mitogen-activated protein kinase
BSA	Bovine serum albumin
PRM	Protamine
HPLC	High-performance liquid chromatography
FA	Folic acid
LI	Labeling indexes

Supplementary Information

The online version contains supplementary material available at https://doi.org/10.1186/s12645-023-00229-z.

Additional file 1: **Fig. S1.** Growth curves of mice in different groups during experimental weeks. **Table S1.** Means of the Initial, Final Body, Absolute and Relative Organ Weights and Weight gains. **Fig. S2.** Log curves of qRT-PCR melting, raw, and quantitation data in Cycling A. Green for mRNA expressions of *HRAS* **(A–C)**, *MAPK* **(D–F)**, and *Bcl2* **(G–I)** in animal lung cancer mouse. **Fig. S3.** Log curves of qRT-PCR melting, raw, and quantitation data in Cycling A. Green for mRNA expressions of *Bax* **(J–L)**, *P21* **(M–O)**, and *B-actin* housekeeping gene **(P–R)** in animal lung cancer mouse.

Salim *et al. Cancer Nanotechnology*　(2023) 14:77

Page 20 of 21

Availability of data and materials
Data are available in a publicly accessible repository.

Declarations

Ethics approval and consent to participate
All experiments were conducted in accordance with the US National Institutes of Health Guidelines for the Care and Use of Laboratory Animals and Cell Line Experiments Guide for the Care and Use of Laboratory Animals after being approved by the relevant Ethical Committee and authorized by the Italian and German Ministry of Health. This study was also approved by the Research Ethics Committee for Institutional Animal Care and Use of Tanat University (IACUC/SCI/TU: 0129).

Consent for publication
All authors have provided their agreement to publish the submitted manuscript.

Competing interests
The authors declare no conflict of interest.

References
Abdella E, Tohamy A, Ahmad R (2009) Antimutagenic activity of Egyptian propolis and bee pollen water extracts against cisplatin-induced chromosomal abnormalities in bone marrow cells of mice. Int J Cancer Manag 2(4):e80637

Abdel-Raouf N, Alharbi RM, Al-Enazi NM, Alkhulaifi MM, Ibraheem IBM (2018) Rapid biosynthesis of silver nanoparticles using the marine red alga Laurencia catarinensis and their characterization. Beni-Suef Univ J Basic Appl Sci 7:150–157. https://doi.org/10.1016/j.bjbas.2017.10.003

Akbal O, Bolat G, Yaman YT, Abaci S (2020) Folic acid conjugated Prussian blue nanoparticles: synthesis, physicochemical characterization and targeted cancer cell sensing. Colloids Surf B Biointerfaces 187:110655. https://doi.org/10.1016/j.colsurfb.2019.110655

Bear HD, Tang G, Rastogi P, Geyer CE Jr, Liu Q, Robidoux A, Baez-Diaz L, Brufsky AM, Mehta RS, Fehrenbacher L (2015) Neoadjuvant plus adjuvant bevacizumab in early breast cancer (NSABP B-40 [NRG Oncology]): secondary outcomes of a phase 3, randomised controlled trial. Lancet Oncol 16:1037–1048

Ben Bacha A, Norah A-O, Al-Osaimi M, Harrath AH, Mansour L, El-Ansary A (2020) The therapeutic and protective effects of bee pollen against prenatal methylmercury induced neurotoxicity in rat pups. Metab Brain Dis 35:215–224

Berk Ş, Kaya S, Akkol EK, Bardakçı H (2022) A comprehensive and current review on the role of flavonoids in lung cancer–experimental and theoretical approaches. Phytomedicine 98:153938. https://doi.org/10.1016/j.phymed.2022.153938

Ferguson LR (2001) Role of plant polyphenols in genomic stability. Mutat Res 475(1–2):89–111. https://doi.org/10.1016/s0027-5107(01)00073-2

Fujimoto J, Wistuba II. Current concepts on the molecular pathology of non-small cell lung carcinoma. In: Proceedings of the Seminars in diagnostic pathology, 2014; pp. 306–313.

Govindan R, Page N, Morgensztern D, Read W, Tierney R, Vlahiotis A, Spitznagel EL, Piccirillo J (2006) Changing epidemiology of small-cell lung cancer in the United States over the last 30 years: analysis of the surveillance, epidemiologic, and end results database. J Clin Oncol 24:4539–4544

Granja A, Pinheiro M, Reis S (2016) Epigallocatechin Gallate Nanodelivery Systems for Cancer Therapy. Nutrients. https://doi.org/10.3390/nu8050307

Hanafy NAN, Salim EI, Mahfouz ME, Eltonouby EA, Hamed IH (2022) Fabrication and characterization of bee pollen extract nanoparticles: their potential in combination therapy against human A549 lung cancer cells. Food Hydrocoll Health. https://doi.org/10.1016/j.fhfh.2022.100110

Hanafy NAN, Eltonouby EAB, Salim EI, Mahfouz ME, Leporatti S, Hafez EH (2023) Simultaneous administration of bevacizumab with bee-pollen extract-loaded hybrid protein hydrogel NPs is a promising targeted strategy against cancer cells. Int J Mol Sci 24(4):3548. https://doi.org/10.3390/ijms24043548

Howlader N, Noone A, Krapcho M, Miller D, Brest A, Yu M, Ruhl J, Tatalovich Z, Mariotto A, Lewis D (2019) SEER cancer statistics review, 1975–2016. National Cancer Institute, Bethesda

Hsu S-M, Raine L, Fanger H (1981) Use of avidin-biotin-peroxidase complex (ABC) in immunoperoxidase techniques: a comparison between ABC and unlabeled antibody (PAP) procedures. J Histochem Cytochem 29:577–580

Hu C-MJ, Aryal S, Zhang L (2010) Nanoparticle-assisted combination therapies for effective cancer treatment. Ther Deliv 1:323–334

Karimi Jashni H, Kargar Jahromi H, Bagheri Z (2016) The effect of palm pollen extract on polycystic ovary syndrome (POS) in rats. Int J Med Res Health Sci 5:317–321

Keskin M (2022) Synthesis, characterization and antidiabetic potential of bee pollen based silver nanoparticles. El-Cezeri 9:266–275

Khan AU, Dagur HS, Khan M, Malik N, Alam M, Mushtaque M (2021) Therapeutic role of flavonoids and flavones in cancer prevention: current trends and future perspectives. Eur J Med Chem Reports 3:100010

Khodapasand E, Jafarzadeh N, Farrokhi F, Kamalidehghan B, Houshmand M (2015) Is Bax/Bcl-2 ratio considered as a prognostic marker with age and tumor location in colorectal cancer? Iran Biomed J 19:69

Kim D, Maharjan P, Jin M, Park T, Maharjan A, Amatya R, Yang J, Min KA, Shin MC (2019) Potential albumin-based antioxidant nanoformulations for ocular protection against oxidative stress. Pharmaceutics 11:297

Koboziev I, Karlsson F, Zhang S, Grisham MB (2011) Pharmacological intervention studies using mouse models of the inflammatory bowel diseases: translating preclinical data into new drug therapies. Inflamm Bowel Dis 17(5):1229–1245. https://doi.org/10.1002/ibd.21557

Kumar B, Smita K, Angulo Y, Debut A, Cumbal L (2022) Honeybee pollen assisted biosynthesis of nanogold and its application as catalyst in reduction of 4-nitrophenol. Heliyon 8:e10191. https://doi.org/10.1016/j.heliyon.2022.e10191

Kwon MC, Berns A (2013) Mouse models for lung cancer. Mol Oncol 7(2):165–177. https://doi.org/10.1016/j.molonc.2013.02.010

Liu WC, Ballenger B, Algarni A, Velez M (2017) FTIR characterization and release of bovine serum albumin from bioactive glasses. J Appl Biomater Funct Mater 15:e347–e355. https://doi.org/10.5301/jabfm.5000374

Medeiros K, Figueiredo C, Figueredo T, Freire K, Santos F, Alcântara-Neves NM, Silva T, Piuvezam M (2008) Anti-allergic effect of bee pollen phenolic extract and myricetin in ovalbumin-sensitized mice. J Ethnopharmacol 119:41–46

Naseri L, Khazaei MR, Khazaei M (2021) Potential therapeutic effect of bee pollen and metformin combination on testosterone and estradiol levels, apoptotic markers and total antioxidant capacity in a rat model of polycystic ovary syndrome. Int J Fertil Steril 15:101–107. https://doi.org/10.22074/ijfs.2020.134604

Padanad MS, Konstantinidou G, Venkateswaran N, Melegari M, Rindhe S, Mitsche M, Yang C, Batten K, Huffman KE, Liu J (2016) Fatty acid oxidation mediated by Acyl-CoA synthetase long chain 3 is required for mutant KRAS lung tumorigenesis. Cell Rep 16:1614–1628

Parashar P, Tripathi CB, Arya M, Kanoujia J, Singh M, Yadav A, Kumar A, Guleria A, Saraf SA (2018) Biotinylated naringenin intensified anticancer effect of gefitinib in urethane-induced lung cancer in rats: favourable modulation of apoptotic regulators and serum metabolomics. Artif Cells Nanomed Biotechnol 46:S598–S610

Park T, Lee S, Amatya R, Cheong H (2020) ICG-loaded PEGylated BSA-silver nanoparticles for effective photothermal cancer therapy. Int J Nanomedicine 15:5459–5471. https://doi.org/10.2147/ijn.s255874

Ragelle H, Crauste-Manciet S, Seguin J, Brossard D, Scherman D, Arnaud P, Chabot GG (2012) Nanoemulsion formulation of fisetin improves bioavailability and antitumour activity in mice. Int J Pharm 427:452–459

Renault-Mahieux M, Mignet N, Seguin J, Alhareth K, Paul M, Andrieux K (2022) Co–encapsulation of flavonoids with anti–cancer drugs: A challenge ahead. Int J Pharm 623:121942. https://doi.org/10.1016/j.ijpharm.2022.121942

Ruseska I, Fresacher K, Petschacher C, Zimmer A (2021) Use of protamine in nanopharmaceuticals–a review. Nanomaterials (basel). https://doi.org/10.3390/nano11061508

Saisavoey T, Sangtanoo P, Chanchao C, Reamtong O, Karnchanatat A (2021) Identification of novel anti-inflammatory peptides from bee pollen (*Apis mellifera*) hydrolysate in lipopolysaccharide-stimulated RAW264.7 macrophages. J Apicult Res 60:280–289

Salim EI, Aboueisha SS, Khamis AA (2022) Balanitoside as a natural adjuvant to gemcitabine in lung cancer experimental model. Nutr Cancer 74(9):3388–3402

Singh S, Aswath MU, Das Biswas R, Ranganath RV, Choudhary HK, Kumar R, Sahoo B (2019) Role of iron in the enhanced reactivity of pulverized Red mud: Analysis by Mössbauer spectroscopy and FTIR spectroscopy. Case Stud Constr Mater 11:e00266. https://doi.org/10.1016/j.cscm.2019.e00266

Sung H, Ferlay J, Siegel RL, Laversanne M, Soerjomataram I, Jemal A, Bray F (2021) Global cancer statistics 2020: GLOBOCAN estimates of incidence and mortality worldwide for 36 cancers in 185 countries. CA Cancer J Clin 71:209–249

Swiatly-Blaszkiewicz A, Pietkiewicz D (2021) Rapid and accurate approach for honeybee pollen analysis using ED-XRF and FTIR spectroscopy. Molecules. https://doi.org/10.3390/molecules26196024

Travis WD, Brambilla E, Nicholson AG, Yatabe Y, Austin JH, Beasley MB, Chirieac LR, Dacic S, Duhig E, Flieder DB (2015) The 2015 World Health Organization classification of lung tumors: impact of genetic, clinical and radiologic advances since the 2004 classification. J Thorac Oncol 10:1243–1260

Turosov V, Mohr U. editors, Pathology of tumours in laboratory animals. Vol. 2: Tumours of the mouse. Chapter: Tumours of the lungs. IARC scientific publication No. 111. Lyon, France, 1990. 325–55. ISBN-13.978-92-832-2111-1.

Vindeløv LL (1977) Flow microfluorometric analysis of nuclear DNA in cells from solid tumors and cell suspensions. Virchows Archiv B 24:227–242

Xie M, Zhang J, Tschaplinski TJ, Tuskan GA, Chen JG, Muchero W (2018) Regulation of Lignin Biosynthesis and Its Role in Growth-Defense Tradeoffs. Front Plant Sci 9:1427. https://doi.org/10.3389/fpls.2018.01427

Zakhireh S, Omidi Y, Beygi-Khosrowshahi Y, Barzegari A, Barar J, Adibkia K (2022) Synthesis and biological impacts of pollen shells/Fe3O4 nanoparticles composites on human MG-63 osteosarcoma cells. J Trace Elem Med Biol 71:126921. https://doi.org/10.1016/j.jtemb.2022.126921

Zaritskaya L, Shafer-Weaver KA, Gregory MK, Strobl SL, Baseler M, Malyguine A (2009) Application of a flow cytometric cytotoxicity assay for monitoring cancer vaccine trials. J Immunother 32:186–194

Zheng X, Pan D, Zhu G, Zhang L, Bhamra A, Chen R, Zhang H, Gong Q, Gu Z, Luo K (2022) A dendritic polymer-based nanosystem mediates drug penetration and irreversible endoplasmic reticulum stresses in tumor via neighboring effect. Adv Mater 34:2201200

Publisher's Note